Automatic Rotational Viscometer and High-Pressure Apparatus for the Study of the Non-Newtonian Behavior of Materials

A. F. GABRYSH, H. EYRING, SHAO-MU MA, AND KAI LIANG

Institute for the Study of Rate Processes and Department of Metallurgy, University of Utah, Salt Lake City, Utah

The automatic concentric-cylinder rotational viscometer described here records flow curves of shear stress versus rate of shear. It provides an automatic means of increasing and decreasing the applied rates of shear and an automatic control of the time that each shear rate is applied to the sample. In as much as flow properties may change rapidly with time and shear rates, this automatic control is important for materials which are time dependent. Presently, with proper selection of the axle and transmission gears, the cup's rotational speed can be automatically varied from zero to 1830 rpm. A switch permits the operator to select a constant shear rate and record shearing stress changes as a function of time at any point of this range. By simply replacing the gear sets, a speed of approximately 2750 rpm can be achieved. The time required for the speed to change from zero to a preset maximum, at constant acceleration, is controlled by voltage changes through a Variac which affords a continuous range from 11 to 300 sec. Shear rates of up to 4090 sec^{-1} are obtained. The cup and bob are aligned coaxially and mechanically fixed. Added cup-bob features for bob-flushing effectively control effects of frictional heating within the sample. Other apparatus described here provides a means to measure the consistency of greases, near the "pseudo solidification" point induced by high pressures. The flow curves of greases which have a critical solidifying pressure reveal characteristics suggesting stiffer consistencies at increasingly high pressures. A 6-tank "reservoir" of hydraulic fluid is used where the fluid under compression and the tensile stresses in the steel of the tanks are used to completely eliminate the antagonistic "ripples" in the pressure which are caused by the action of the pump. Pressures of 0–50 000 psi are easily and safely obtainable with this apparatus.

I. AN AUTOMATIC CONCENTRIC-CYLINDER ROTATIONAL VISCOMETER FOR RHEOLOGICAL MEASUREMENTS OF NON-NEWTONIAN FLOW

INTRODUCTION

AMONG the various types of viscometers, the rotational viscometer is one of the more commonly used instruments for measuring viscosities. It consists of two concentric cylinders, and the liquid to be tested is contained in the annular space between the two cylinders. Either the external (Couette type) or the internal cylinder (Searle type) is rotated, while the other is kept in position. The viscometer reported here belongs to the Couette type. Although the principle of the Couette type viscometer is well known, a brief description is given below, since it will serve for a better understanding of its use, especially for non-Newtonian fluids.

1. Variables for Newtonian Flow

When the cup (external cylinder) is rotated the liquid is sheared in the annular space, and attains a steady state for a given angular velocity. The torque acting on every molecular layer of the liquid is the same, otherwise the condition of the steady state does not hold.[1] The torque on a molecular layer located at a distance r from the common axis is given by τ and it should be the same as the torque acting on the surface of the bob (internal cylinder). The total torque (measured by a transducer) is given by

$$\tau = 2\pi r^2 h f, \tag{1}$$

where h is the height of the bob immersed in the liquid, or an equivalent height if there are end effects, and f is the

shear stress (force per unit area) acting on the molecular layer under consideration. Under a shear stress f successive molecular layers shear with respect to the neighboring layer. The rate of shear (velocity gradient) $\dot{s}$ is given by

$$\dot{s} = dv/dr = r(d\omega/dr), \tag{2}$$

where v is the linear velocity and ω is the angular velocity. Generally, $\dot{s}$ is a function of f, i.e.,

$$\dot{s} = F(f) = r(d\omega/dr). \tag{3}$$

From Eq. (1), $dr/r = -df/2f$; substituting into Eq. (3) one obtains

$$\omega = \int_{\omega=0}^{\omega} d\omega = -\frac{1}{2}\int_{f_b}^{f} F(f)\frac{df}{f}. \tag{4}$$

Here, $f_b(=\tau/2\pi R_b^2 h$, where R_b is the radius of the bob) is the shear stress on the surface of the bob, and $f(=\tau/2\pi r^2 h)$ is the stress on the representative molecular layer a distance r from the axis of the bob.

For Newtonian fluids, the relation, $F(f) = f/\eta$, ($\eta =$ viscosity, which is independent of f or $\dot{s}$), is introduced into Eq. (4) and by integrating the latter from f_b to f_c (shear stress on the surface of the cup), one obtains

$$\Omega = \frac{\tau}{4\pi\eta h}\left[\frac{1}{R_b^2} - \frac{1}{R_c^2}\right], \tag{5}$$

where $\Omega = 2\pi n/60$, n being rpm (revolutions per minute). From Eqs. (1) and (5) one obtains

$$\eta = f_b \Bigg/ \frac{4\pi n}{60[1 - (R_b^2/R_c^2)]}. \tag{6}$$

Defining η as $f/\dot{s}$, the f and $\dot{s}$ on the bob surface are

$$f = \tau/2\pi R_b^2 h \tag{7}$$

---

[1] M. Reiner, *Deformation and Flow* (H. K. Lewis and Company Ltd., London, 1949), pp. 27–34.

and

$$\dot{s} = 2\Omega/(1-\alpha^2) = 4\pi n/60(1-\alpha^2), \qquad (8)$$

where

$$\alpha \equiv R_b/R_c.$$

Reiner,[1] Philippoff,[2] and Green[3] fully develop Eqs. (6), (7), and (8) for Newtonian liquids.

2. Variables for Non-Newtonian Flow

For non-Newtonian fluids, the integration of Eq. (4) is more difficult than shown above, since η in $F(f)$ $[=f/\eta]$ is a function of f or $\dot{s}$. Here $\dot{s}[=F(f)]$ is calculated as follows. For non-Newtonian fluids, (4) yields

$$\Omega = -\frac{1}{2}\int_{f_c/\alpha^2}^{f_c} F(f)df/f, \qquad (9)$$

where f_b has been replaced by f_c/α^2 from the relation

$$R_b^2/R_c^2 = f_c/f_b = \alpha^2 \qquad (10)$$

which is derived from Eq. (1). From Eq. (9) one gets

$$[\partial\Omega/\partial\alpha]_{f_c} = -F(f_b)/\alpha. \qquad (11)$$

The quantities, f and $\dot{s}$, given by Eqs. (7) and (8) are exactly calculable even for non-Newtonian fluids. The apparent fluidity ϕ_{ap} is defined as

$$\phi_{ap} = 2\Omega/f_b(1-\alpha^2) \qquad (12)$$

giving

$$\Omega = -\tfrac{1}{2}\phi_{ap}f_c(1-1/\alpha^2). \qquad (13)$$

Introducing $(\partial\Omega/\partial\alpha)_{f_c}$, from (13) into (11) one gets

$$\frac{F(f_b)}{f_b} = \phi_{ap} + \tfrac{1}{2}\alpha(\alpha^2-1)\left[\frac{\partial\phi_{ap}}{\partial\alpha}\right]_{f_c} \qquad (14)$$

which is readily transformed to

$$F(f_b) = f_b\phi_{ap}\{1+\Delta(f)\} = \frac{2\Omega}{1-\alpha^2}\{1+\Delta(f)\}, \qquad (15)$$

where

$$\Delta(f) = \left[\frac{\partial \ln\phi_{ap}}{\partial \ln(1-1/\alpha^2)}\right]_{f_c}. \qquad (16)$$

The relation (15) shows that when $\Delta(f)\ll 1$ the shear rate, $\dot{s} = [F(f_b)]$, is given by (8). Thus, $\Delta(f)$ is the correction,[4]

for the non-Newtonian behavior of the liquid, which was studied by several investigators.[5–10]

The correction $\Delta(f)$ is obtained by measuring ϕ_{ap} at a constant f_c with cylinders of various α. Since the method using many cylinders is very inconvenient, two methods have been devised[7]: one uses two bobs with one cup (the double bob method), and the other uses only one bob with one cup (the single bob method). The details of these methods are given by Krieger.[6]

Even for non-Newtonian fluids, $\dot{s}$ is calculated using Eq. (8), since the $\Delta(f)$ is frequently within 10% of the Newtonian $\dot{s}$. For exact studies, however, $\dot{s}$ should be calculated from Eq. (15).

Occasional slippage occurs on the surfaces of the cup and bob. The correction for the slippage effect was studied by Mooney.[5] If slippage is evident, the corresponding correction should be incorporated in calculating Ω, before the above $\Delta(f)$ correction is made.

3. Shortcomings of the Rotational Viscometer

The Green–Weltmann type of viscometer[2,11] is convenient for studying thixotropic and rheopectic (dilatant) substances. However, it also has formidable shortcomings. Among others, the temperature rise due to frictional heating was frequently criticized.[12,13] For example, Lower, Walker, and Zettlemoyer[12] found that heavy mineral oil did not show a thixotropic hysteresis loop when it was studied in an apparatus where the temperature was carefully controlled, while Weltmann[14] found a thixotropic loop in her experiment using the rotational viscometer (Couette type). Thus, the authors claimed that the hysteresis loops found by Green and Weltmann are not due to thixotropy (structural breakdown), but due to softening of the materials caused by the rise in temperature. However, Hahn[15] showed their concept is only partly right, since some thixotropic substances are destroyed by a very small mechanical disturbance.

In view of the fact that the frictional heating plays a large role in viscosity studies, careful attention was paid to minimize this effect in constructing the viscometer. Water from the thermostat, in which the cup-bob part of the viscometer was immersed, was circulated through the

[2] W. Philippoff, *Viskosität der Kolloide* (Verlag von Theodor Steinkopff, Dresden und Leipzig, 1942).
[3] H. Green, *Industrial Rheology and Rheological Structures* (John Wiley & Sons, Inc., New York, 1949).
[4] Equation (15) is similar to an equation originally derived by Rabinowitsch for non-Newtonian flow in a capillary. The original derivation was modified by Saal and Koens. Later the correction Δf was studied first by Mooney, later by Krieger and Maron, and by Fritz and Kroepelin. The final form of the original (Rabinowitsch) equation, given by (15), is due to the work of Krieger and Maron.

[5] M. Mooney, J. Rheology 2, 210 (1931).
[6] I. M. Krieger and S. H. Maron, J. Appl. Phys. 23, 147 (1952).
[7] W. Fritz and H. Kroepelin, Kolloid-Z. 140, 149 (1955).
[8] R. Rabinowitsch, Z. Physik. Chem. A145, 1 (1929).
[9] R. N. J. Saal and G. J. Koens, Inst. Petroleum Tech. 19, 176 (1933).
[10] I. M. Krieger and S. H. Maron, J. Appl. Phys. 25, 72 (1954).
[11] R. H. Weltmann, N. L. G. I. Spokesman 20, No. 3, 34 (1956).
[12] G. W. Lower, W. C. Walker, and A. C. Zettlemoyer, J. Colloid Sci. 8, 119 (1953).
[13] R. N. Weltmann, Ind. Eng. Chem. 40, 272 (1948).
[14] R. N. Weltmann, J. Appl. Phys. 14, 343 (1943).
[15] S. J. Hahn, T. Ree, and H. Eyring, N. L. G. I. Spokesman 23, 129 (1959).

inside of the bob where thermocouples are incorporated. Some preliminary results[16,17] are quite good.

In the following, a precise description of the viscometer is given, and an example of experimental results on a rheopectic substance is reported.

CONSTRUCTION

1. General

The general and detailed features of the viscometer may be seen in Figs. 1 to 4. The "cup" or outer cylinder of the cylinder assembly (Fig. 3) is rotated through a variable speed transmission by a motor. The sample is sheared between the two coaxial cylindrical surfaces of the cup and bob [Fig. 3(b)]. The torque on the bob is measured by a Statham "strain gauge" transducer and is recorded as a function of shear rate given by the output of a tachometer which is directly coupled to the variable speed transmission, Fig. 5. The output of the tachometer, or shear rate, is proportional to the rotational speed of the cup. The output of the transducer, or shear stress, is proportional to the torque. The outputs of the transducer and the tachometer are simultaneously plotted by an X–Y recorder, respectively. The recorder curve is a rate-of-shear versus shear stress curve.

2. Temperature-Control Apparatus

The constant-temperature bath and controls are shown in Fig. 2. A Micro-set regulator triggers the thermoregulator control C for current to two (auxiliary and intermittent) heating elements E. At higher than 5°C to about 70°C the temperature is easily controlled within 0.1°C.
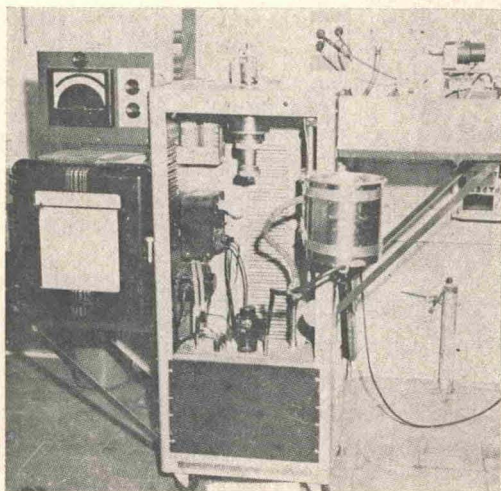
Low temperatures are obtained by passing cold water through the cooling coils D. Temperatures from 1 to 5°C are controlled within 0.3°C. A water pump F circulates water up through the pipe marked "inlet" at the bottom of the water container. The water is returned to the insulated bath through a tube attached at a point near the top of the water bath.

The container is mounted on a spring-loaded slide bar so that it can be easily moved down and out (or in) for changing samples. The bob-flushing system shown more clearly in Fig. 3 affords better control of the temperature of the sample being sheared. Heat is transferred from the sample to the water and carried away. A soft rubber truncated cone, Fig. 4, drawn over the top of the bob shaft in such a way as not to make contact with the system, deflects the over-flowing water into a "catch-cup" from which it is directed through a tube back into the bath. The amount of water which passes through the bob-flushing system is easily regulated.

After the entire system has gained equilibrium, usually about 30 min, shearing is begun and the differences in the temperature of the water, as it enters and leaves the system, is noted as related to the temperature changes in the sample due to friction during shearing.

In order to gain a more dependable record of temperature changes in the sample during shearing, thermocouples isolated from the flushing water were placed at points shown in Fig. 4. Differential temperature changes between
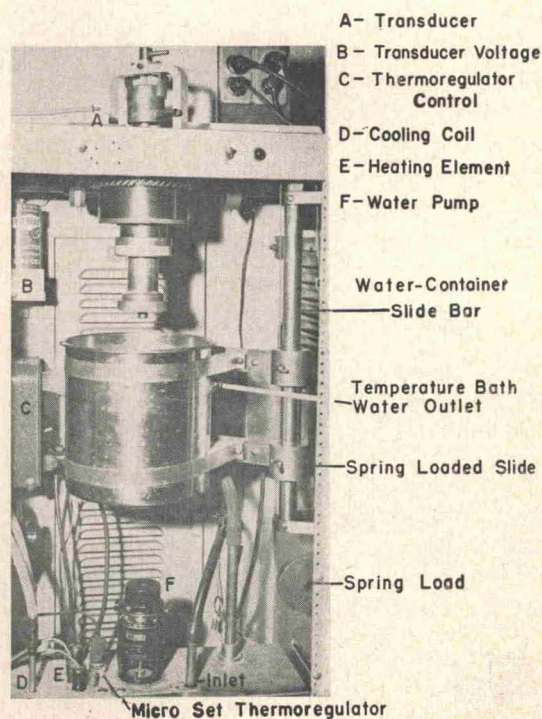

FIG. 1. Photograph of viscometer.

[16] A paper presented at the 137th Annual Meeting of the American Chemical Society (1960).
[17] D. Miles and H. Eyring, "Flow Properties and Frictional Heating Effects in Lubricating Grease" (to be published).

A– Transducer
B – Transducer Voltage
C– Thermoregulator Control
D– Cooling Coil
E– Heating Element
F– Water Pump

Water-Container
Slide Bar

Temperature Bath
Water Outlet

Spring Loaded Slide

Spring Load

Micro Set Thermoregulator

FIG. 2. Photograph of temperature control system.

the bob's thermocouples and another thermocouple placed in the bath water are recorded.

3. Rotating Mechanism

The photograph of Fig. 3 and the diagram of Fig. 4 show the cylinder assembly and rotating parts. Figure 4 shows the coaxial alignment of the cup and bob and the gearings in detail. The axes of the two cylinders are maintained parallel, mechanically, through four sets of ball bearings by a bearing holder which keeps the cylinders permanently coaxially aligned. All bearing areas are "sealed" from circulating air by "dust stops." A conical shoulder on the cup and a flat shoulder on the mounting cylinder provide bearing surfaces by which the concentricity of the cup and bob is repeated after each removal of the cup.

The mounting cylinder, to which the cup is mechanically and coaxially fixed, is driven by means of the "cup gear" at speeds varying with the selection of the fixed gears (discussed in the following section) between cup and motor.

CALIBRATION AND RECORDING

1. Shear Rates

Figure 5 shows the location of the direct couplings, the driving shaft, and the helical driving gears. The rotational speed of the driving motor is 3450 rpm. A variable speed (Graham) transmission reduces this speed to a range of 0 to 1100 rpm at the "drive position." The cup can be driven at speeds continuously varying from 0 to 2750 rpm, depending on the selection of gear combination made according to the gear schedule given in Table I.

The velocity of the transmission is regulated by a Variac controlled Dumore motor which is belt-pulley coupled to the transmission (see mounting on right-hand side of viscometer in Fig. 1). Automatic tripping of Micro Switches permits continuous cycling from zero shear rate to the
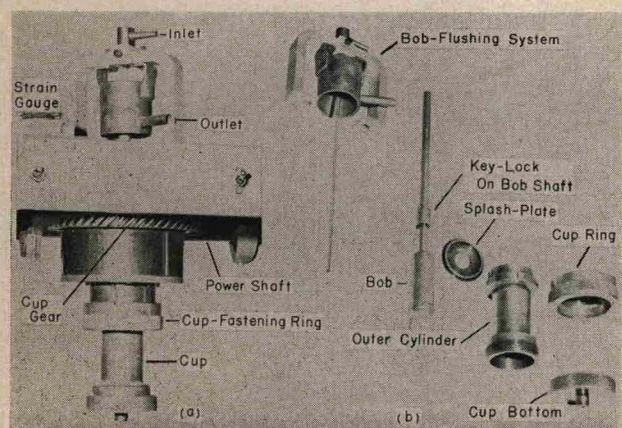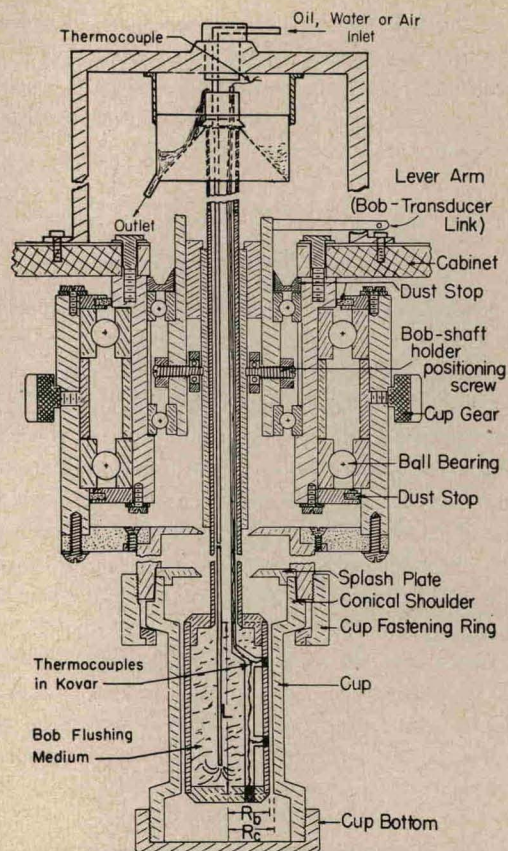

FIG. 4. Schematic of cylinder and cup-bob assembly with temperature control system.

selected maximum. Varying the voltage to the Dumore motor enables one to change the transmission acceleration so that the time required to increase the shear rate from zero to any selected maximum speed can vary continuously from 11 to 300 sec. The calibration dial makes the speed setting reproducible within 1.0%.

A calibrated "speed meter" is mounted above the recorder (Fig. 1) and is energized, simultaneously with the recorder, by voltages from the tachometer-generator. The meter provides a visual aid to controlling the shear rate
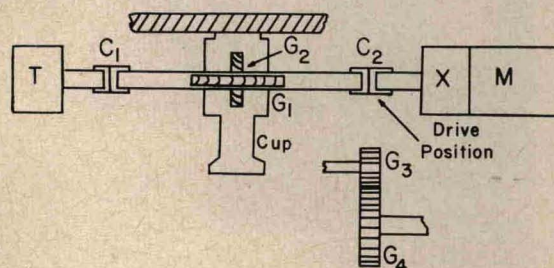

FIG. 3. Photograph of (a) rotating cylinder and (b) cup-bob assembly.

FIG. 5. Schematic of relative location of fixed gear and direct-couple: T—tachometer; C_1—flexible coupling; G_1 and G_2—relative positions of helical (45°) gears 1 and 2; C_2—Boston gear coupling (FCBB type); G_3—axial gear; G_4—transmission gear; M—motor; X—variable speed transmission, (a) input rpm—3450, (b) output rpm—1100 to 0.

TABLE I. Gear schedule and cup speeds.

Gear set	Position	Gear	At drive position Axel gear	At drive position Transmission gear	Calculated at cup	Maximum rpm Motor—3450 rpm Tachometer—100 rpm Measured at tachometer	Measured at cup[a]	Maximum shear rate (sec⁻¹) Cylinder set #1 $\dot{s}=(0.965n)$	Cylinder set #2 $\dot{s}=(2.245n)$
	1	48	Direct		367	1092±6	362±2	349	809
1	2	16	couple						
	1	48	Direct		733	1092±6	730±3	704	1632
2	2	32	couple						
	1	48	Direct		1100	1092±6	1097±3	1062	2459
3	2	48	couple						
	1	48	Na16B	NA20B	458	1092±6	455±3	439	1017
1	2	16		NA40B	917		911±3	879	2036
	1	48	NA16B	NA20B	917	1092±6	911±3	879	2036
2	2	32		NA40B	1833		1830±6	1766	4090
	1	48	NA16B	NA20B	1375	1092±6	1370±5	1327	3073
3	2	48		NA40B	2750		2750±10	2654	6146

[a] Using maximum rpm *measured* at cup.

build up. It also enables one to switch to a "hold" (constant shearing) at any desired shear rate. The resistor above the speed meter (R_4 in Fig. 9) controls the needle's maximum deflection for different maximum shear rates. The resistor labeled Y controls the Y axis of the recorder and enables one to expand or compress the Y component (shear rate) of the flow curve.

An "auxiliary" tachometer was used to calibrate the viscometer's tachometer and cup rpm. Figure 6(a) gives the tachometer-meter readings, with a direct couple at the drive position, for the helical gear sets 1 and 2 (Table I).
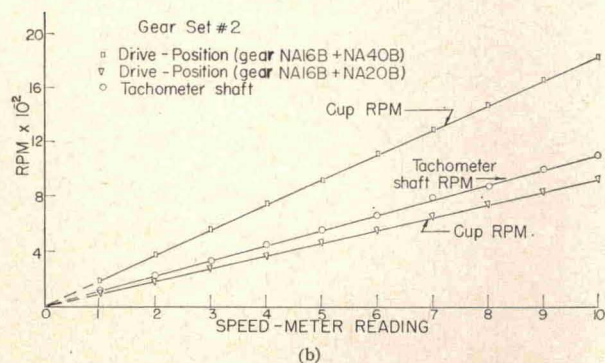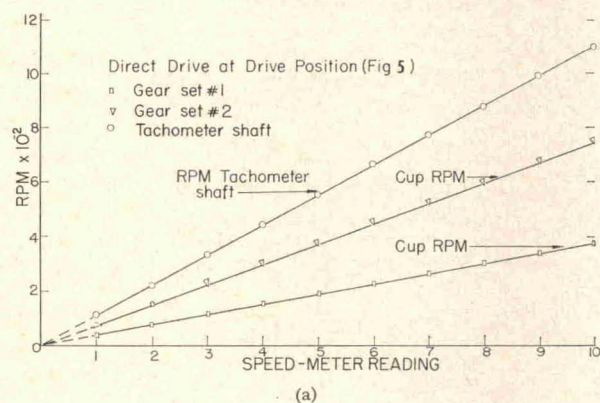

FIG. 6. Calibration of speedmeter readings versus rpm for two sets of gears at drive position.

The difference between the rpm at the tachometer shaft and that at the cup results from the ratio of helical gear G_1 to G_2 (Fig. 5).

Figure 6(b) gives the meter calibration for various rpm when using helical gear set #2 at the G_1-G_2 positions, and the noted gear combinations at the drive position. Table I gives the measured rpm maxima.

2. Cylinder Sets

Two cylinder sets consisting of one cup and two bobs are designed (Fig. 4) with the dimensions given in Table II. This design keeps the end effects negligible. The appreciable enlargement of the cup diameter at both ends of the meaningful length h of the annalus makes "outside" forces negligible when compared with the forces exerted on the bob within length h.

Streamline flow in the cylinder involves the orderly motion of liquid in circular paths concentric with the cylinder, with velocities increasing from zero at the surface of the bob to a maximum at the cup. The clearance between cup and bob (R_c-R_b) is kept as small as possible since (a) the distribuiton of shear stress within the material being sheared varies inversely with the square of the radius and (b) heat dissipation from the sample during shear is more rapid.

The maximum (Re_{max}) Reynolds numbers for the two cylinder sets are given in Table II. The Reynolds numbers Re_{max} are calculated for the rotational speed of 1800 rpm

TABLE II. Dimensions of Reynolds numbers and shearing-stress limits of two cylinder sets.

Cylinder set	R_c (cm)	R_b (cm)	R_c-R_b (cm)	R_b/R_c	h (cm)	$Re_{max}=2\pi n R_c^2 \times[1-(R_b/R_c)]\rho/\eta$[a] ($n=1800$ rpm)
1	1.785	1.580	0.205	0.885	6.89	985
2	1.785	1.700	0.085	0.952	6.89	412

[a] $\eta=0.07$ P, $\rho=1$ g/cm³.

(Gear set #2, Table I). The data indicate that Re_{max} is well within the limits of the critical values for turbulent flow.[18,19] Using Eq. (8) and the ratio of R_b/R_c from Table II, the shear rate $\dot{s}$ is found to be $0.965n$ and $2.235n$ for cylinder sets #1 and #2, respectively, where n is the variable rpm.

3. Transducer Calibration

The output of the transducer reflects the instantaneous torque values for the flow curves which are plotted by the X–Y recorder. The accuracy of the plotted torque depends primarily on the precision of transducer operation, which in turn depends to a large extent on the calibration. Various methods[20] of calibration can be used equally well. One is given below.

The current and voltage available from the transducer for the recorder, Fig. 7, are given by the following equations:

$$I_r = SnE/R_{23}+R_r \qquad (17)$$

$$E_r = SnER_r/R_{23}+R_r. \qquad (18)$$

For $R_r \gg R_{23}$, Eq. (18) becomes

$$E_r = SnE_r. \qquad (19)$$

The values of S (sensitivity), R_{23} (output resistance), and E (excitation voltage) are obtained from the transducer data sheet which is supplied by the manufacturer. R_r is the resistance of the recorder and n is the number of units of the variable for which the output is computed.

Equations (17) and (18) are applied for a current or voltage measuring instrument, respectively. Equation (19) is applied when the voltage measuring instrument is of a high impedance.

In the given calibrating circuit Fig. 7, the resistor R_c can be chosen to give the desired fraction of full range output from the relationship

$$R_c = [(10^6/4nS)-0.5]R_{23}. \qquad (20)$$

The number of scale units n which will be produced by a given value of R_c is given by

$$n = 10^6/4S(R_{23}/R_c+0.5R_{23}). \qquad (21)$$

Following the above calibration, a "response" check should be made on the transducer. Figure 8 gives the responses of two transducers to loading and unloading. No detectible difference for the "up-down curve" is shown, signifying reproducibility of the transducer to greater or

[18] G. I. Taylor, Proc. Roy. Soc. (London), A157, 546 (1936).
[19] G. I. Taylor, Proc. Roy. Soc. (London) A157, 565–578 (1936).
[20] Detailed information on controlling the translation of the force, which is applied to the strain sensitive resistance wires in the transducer, into an exact electrical equivalent can be found in the following "Statham" bulletins and notes: 1. Transducer Element, Bulletin No. 1.0; 2. Selection Table (model G1), Bulletin No. 1.1; 3. Selection Table (model G7), Bulletin No. 1.3; 4. Calibrating Resistors, Bulletin No. 600; 5. Indicating and Recording, Instrument Note No. 4.

R_c= Calibrating resistor
E = Voltage source (as rated)
Terminals 1 and 4 = Power Input
Terminals 2 and 3 = Output To Recorder
$R_{14} = R_{12} + R_{24}$ = Bridge resistance (ohms) between 1 and 4
$R_{23} = R_{24} + R_{13}$ = Bridge resistance (ohms) between 2 and 3
R_1 = Potentiometer (20K – 30K)
R_2 = Wire-wound resistor (~100 R_{23})
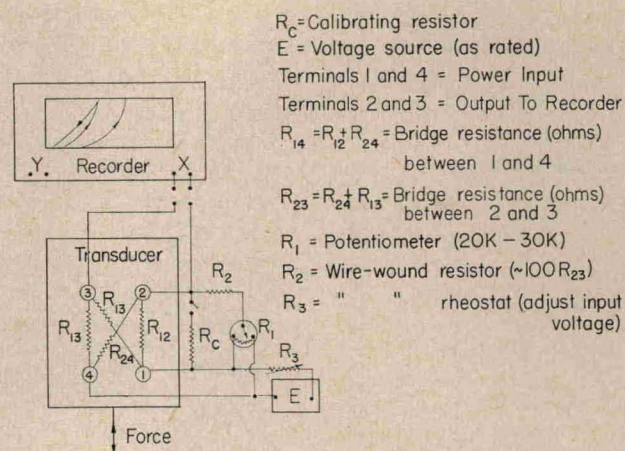R_3 =   "   "   rheostat (adjust input voltage)

FIG. 7. Schematic of circuit for transducer calibration.

lesser shearing force. This check should be made, especially if transducer had been over-loaded.

4. Shear Rate Recording

The drive motor is directly coupled through the transmission by the driving rod, Fig. 5, to a dc model D
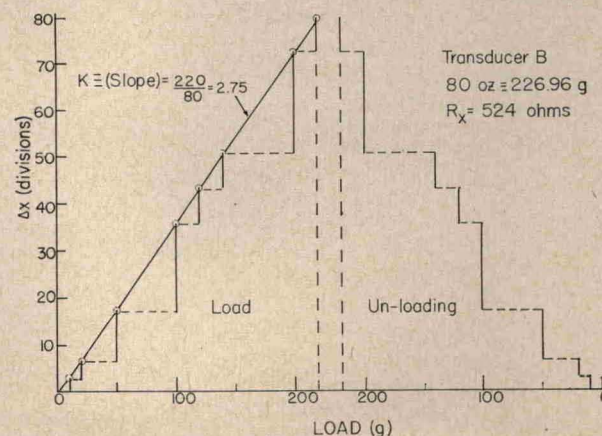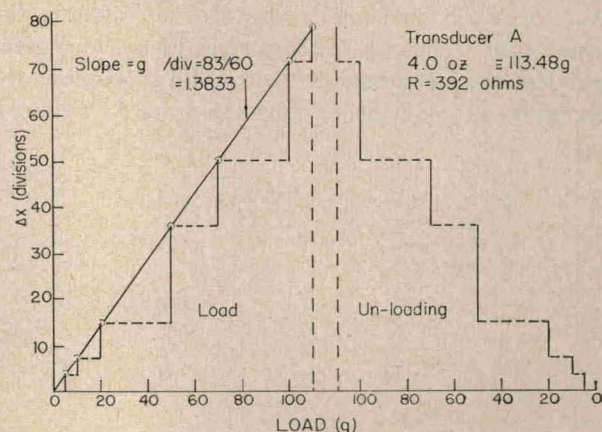
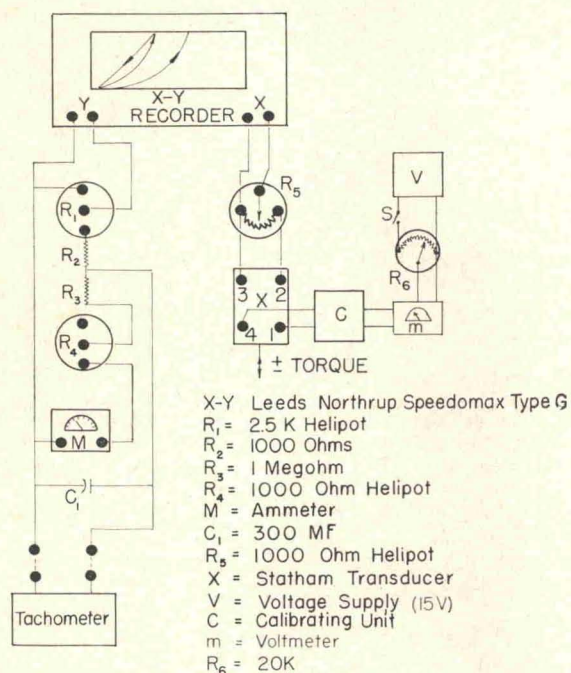FIG. 8. "Histograms" of transducer response to loading and unloading for constants, k.

FIG. 9. Schematic of shear rate and torque recording system (Note: items V, R_6, and M are replaced by Hewlett-Packard model 721A power supply).

X-Y Leeds Northrup Speedomax Type G
R_1 = 2.5 K Helipot
R_2 = 1000 Ohms
R_3 = 1 Megohm
R_4 = 1000 Ohm Helipot
M = Ammeter
C_1 = 300 MF
R_5 = 1000 Ohm Helipot
X = Statham Transducer
V = Voltage Supply (15 V)
C = Calibrating Unit
m = Voltmeter
R_6 = 20K

tachometer generator, obtained from the Esterline-Angus Company, Inc. The internal resistance of the tachometer is 2000 ohms. The maximum desirable armature speed is 1250 rpm. The generator is calibrated, to an accuracy of $1/2\%$, to develop an open circuit emf of 25.0 V at 1000 rpm of the armature. Precise adjustment is made by means of a movable magnetic shunt, attached to the pole pieces, which is capable of varying the generator output over a range of about $\pm3\%$. At the maximum "desirable" armature speed of 1250 rpm the generator develops an open circuit emf of 31.25 V. Since the maximum speed of the transmission is 1100 rpm the direct couple keeps the speed of the armature within the safe range of 1250 rpm maximum. The greater speeds of the cup are achieved by the various gear ratios, Fig. 5 and Table I. The circuit used
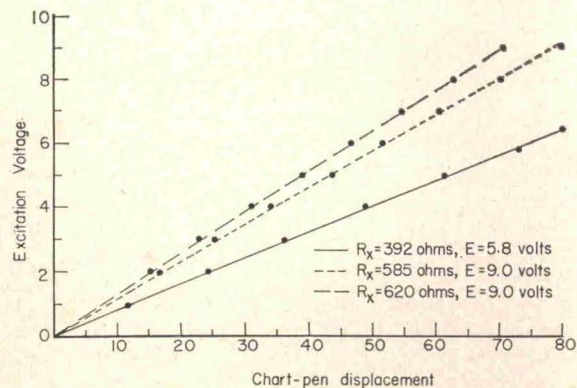

FIG. 10. Recorder-pen deflections versus transducer excitation voltage.

to reduce the output of the tachometer generator to one (about 10 mV), that can be handled by the X–Y recorder, is shown in Fig. 9.

5. Torque Measuring and Recording

Torque is translated into an exact electrical equivalent by means of a complete balanced bridge (Statham transducer) of strain-sensitive resistance wire. Nine units consisting of ±0.15-, ±0.75-, ±1.5-, ±4-, ±8-, ±16-, ±24-, ±32-, and ±80-oz transducers are employed. The excitation voltage for this series of transducers ranges from 8 to 14 V. The above set of transducers and a Hewlett–Packard model 721A dc voltage supply, Fig. 9, permits measurement of forces ranging from about 1 to 2270 g.

After calibrating the transducer (Sec. 3, under Calibration) the deflection of the pen on the chart, for a given applied load to the transducer, can be controlled by either R_5 or R_6 in Fig. 7. When possible it is recommended that the excitation voltage remain that specified for the transducer by the manufacturer and that the upper limit of pen deflection be controlled by R_5. However, if one does find it more convenient to vary R_6 (the excitation voltage) instead of R_5, and because of the linear relationship between voltage and displacement, one can easily correct the data accordingly.

A typical plot of voltage with pen deflection is shown in Fig. 10, for a 4-oz transducer under a constant load but where R_5 or R_6 (excitation voltage) is varied. This plot points out specifically that R_5 and R_6 should have one setting and meter value, respectively, for each transducer, where the recorder is calibrated to full pen deflection at the load limit of the transducer. Subsequent data can then be compared meaningfully.

It has been found desirable to select an "R_5" value so that a near "full load" on the transducer will not cause more than 80 scale divisions (small) on the recorder chart. This affords a rapid check against over-loading which happens often in the case of rheopectic materials where viscosity increases with shear.

The force due to gravity of the bob varies slightly, apparently due to humidity and temperature changes, and is about 0.5 to 0.7 mg. In the 0.15- to 16-oz transducer range, accuracy and linearity of both the transducer and recorder is within 1% of full scale. The 32- and 80-oz transducers show a linearity, with applied torque, within 1.5% of full scale.

The transducers have identical basal dimensions and are easily replaced into an insert of a specially designed plate. The exact position of transducer in relation to the pressure (lever) arm on the bob shaft, Fig. 4, is easily repeated. This position is maintained during measurement.

A force F due to a torque on the bob and translated through the lever arm, Fig. 4, is related to the transducer

by a "machine constant," $C = 67.24$ dyn/cm^2. A transducer constant k, Fig. 8, and the pen deflections Δx (chart divisions) are related to the experimental shear stress f by $f = kC\Delta x$.

EXPERIMENTAL RESULTS

1. Structure

The results reported here were obtained on the mineral attapulgite using a cylinder set #1. With the use of the automatic controls, the viscometer recorded a continuous flow curve in 30 sec with a peak rate of shear of about 700 sec^{-1}.

Figure 11(a) shows the structure of attapulgite as worked out by Bradley.[21] The substitution of Al^{3+} for some of the Si^{4+} is probable, and it is considered that substitution of Al^{3+} for either Mg^{2+} or Si^{4+} or both should weaken the structure.

The chemical analysis (volatile-free basis) of the material (specific gravity 2.36) used in this study is: silicon (SiO_2), 67.0%; aluminum (Al_2O_3), 12.5%; magnesium (MgO), 11.0%; iron (Fe_2O_3), 4.0%; calcium (CaO), 2.5%; other, 3.0%. The bulk density (tamped volume weight) was approximately 0.56 g/cc and the surface area approximately 210 m^2/g on a moisture-free basis. The particle size distribution determined by centrifugal sedimentation is given in Fig. 11(b).

2. Viscometer Calibration

A photograph of a strip of recorder chart, Fig. 12, shows the procedure which was used to record the data. The response of the transducer to loading and unloading is recorded in Fig. 12(a). The "histogram" indicates the accuracy in the response of the transducer to changing load during increasing and decreasing shear rates.

A calibrated 98% glycerol "standard" gave the flow curves shown in Fig. 12(b). The ordinate and abscissa are drawn, only in Fig. 12(b), to show the actual values for
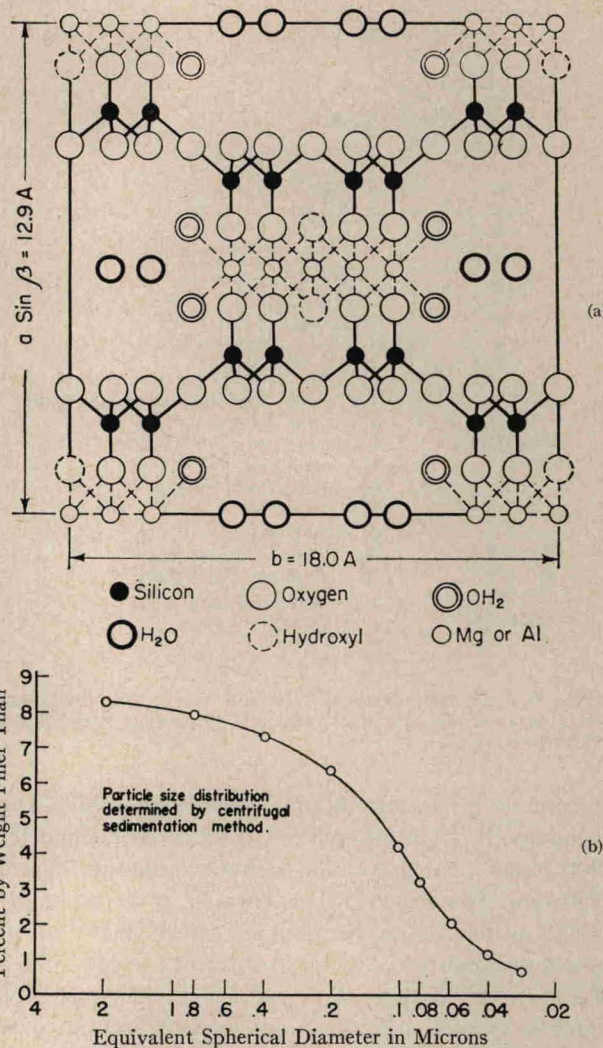
shear rate $\dot{s}$ and shear stress f, respectively. However, these ordinate and abscissa values are the same for the curves in c, d, e, and f. In Fig. 12(b) the up and down

FIG. 11. (a) Structural model of attapulgite and (b) particle size distribution.
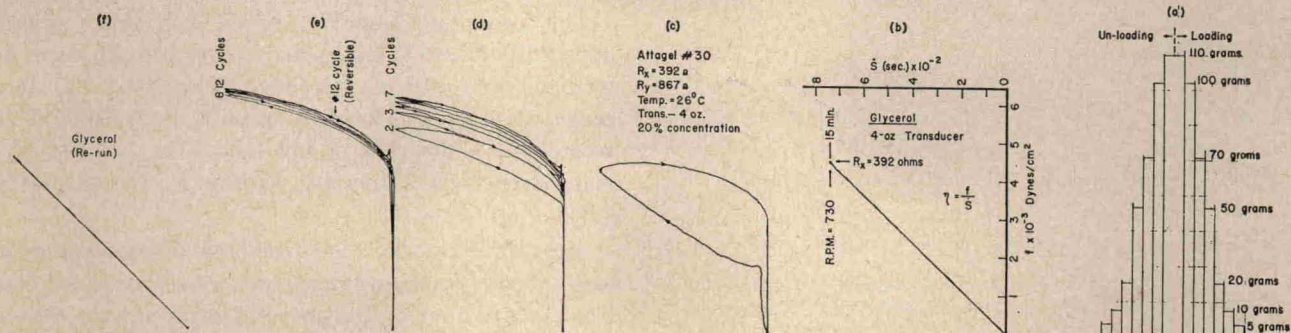
FIG. 12. Experimental procedure: (a) check on transducer response to loading and unloading; (b) calibration with a glycerol standard; (c) first 60-sec cycle for attapulgite suspension in water; (d) decreasing rheopectic loops for successive cycles; (e) continuation of cycling to reversibility; (f) standard re-run for a check on machine operation.

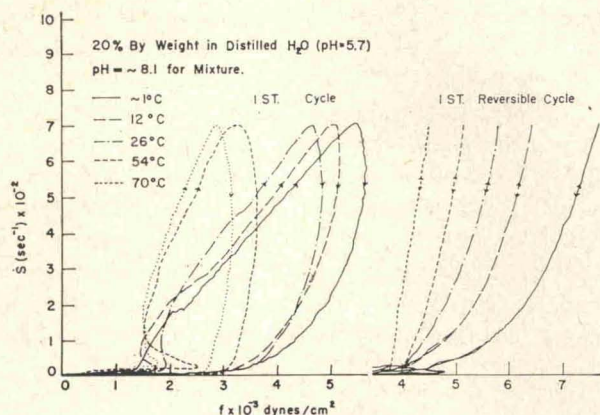[21] W. F. Bradley, Am. Mineralogist **25**, 405 (1940).

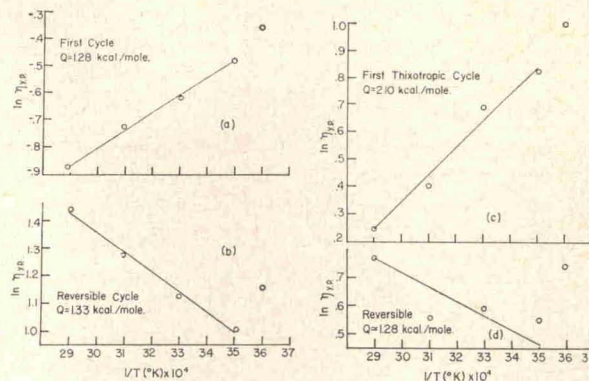FIG. 13. First-cycle and reversible-cycle flow curves for 5 temperatures.

FIG. 14. Temperature dependence of yield-point viscosity for (a) first rheopectic cycle, (b) first reversible cycle, (c) first thixotropic cycle following a 12-h rest period after first reversible cycles were obtained, and (d) second reversible cycle.

curves, both straight lines passing through the origin, coincide; the up and down curves are the flow curves which are obtained while the shear rate is uniformly increased or decreased, respectively. The slope of the straight line in Fig. 12(b) gives the viscosity as $\eta = 6.38$ P at 26°C: this value agrees with the literature value of 6.29.

Figure 12(c) shows a first-cycle rheopectic flow curve which was obtained on attapulgite suspension in water immediately following the "calibration." Successive 60-sec cycles produced the family of curves shown in Fig. 12(d). Complete reversibility was obtained with cycles 10–12, Fig. 12(e), indicating a complete build up of structure. Figure 12(f) shows the results of final recheck of the viscometer, again using the glycerol standard. It confirms proper machine operation during the recording of flow curves shown in Fig. 12(c) to 12(e).

Figure 13 shows the first and reversible-cycle flow curves for attapulgite, at 5 temperatures. In each case the reversible cycles were achieved by successive cycling as in Fig. 12.

3. Fluidity

The entire experimental data[22,23] together with those shown in Figs. 12 and 13 are qualitatively explained on the basis of fluidity being a function of the "free" water available to lubricate particles in suspension. Fluidity depends on (a) time since $\dot{s}$ became zero, (b) shear rate, and (c) amount of surface. At high rates of shear, the majority of the particles are in parallel orientation and water is available to lubricate the slippage of one particle over another; however, this parallel orientation of particles is a state of low entropy. Randomization occurs when the material is held at low shear rates or when there is no shearing action. The nonparallel particles immobilize water, trapping it in the interstices between the cross-linked particles. As the

rate of shear is increased, a yield point is observed when the cross linkage breaks up. With a further increase of shear rate more complete orientation is obtained, water is freed and absorbed on individual particle surfaces. Better lubrication between particles is the result.

4. Activation Energy

The stability of the cross-linked structures obtained with the attapulgite suspension at rest may be observed by plotting the logarithm of the viscosity at the yield point as a function of reciprocal temperature, Fig. 14. The viscosity yield points, Fig. 14(a), are rather low for the first cycles but, where particles are tightly bound in bundles, they follow an exponential relationship as a function of temperature. Yield point viscosities are highest at low temperature where the cross-linked structure is most stable. At high temperatures the thermal activity is sufficient to keep the structure loose and the yield-point viscosity (η_{yp}) is low. The slope of this linear relationship [$\ln\eta_{yp} = f(1/T)$] is a measure of the energy (~ 1.2 kcal/mole) of stability of the cross-linked-type structure. The same explanation holds for the thixotropic condition recorded for the suspension after a twelve hour rest period which followed the first reversible cycle. In this case, however, viscosities at the yield point are much larger because many more individual particles are available following the bundle break up. The energy of stability is about 2.0 kcal/mole, Fig. 14(c).

The speed with which the cross-linked structures form may be deduced from the viscosities at the yield point of the suspensions during the reversible cycling, Fig. 14(b) and 14(d). In these cases, the network structure is only partially formed. Thermal energy will allow the random structure to form more rapidly (or to a greater extent if the time interval is fixed) at high temperatures than at low temperatures. With limited time of formation available, the viscosities at the yield point become a measure of the

[22] A. F. Gabrysh, T. Ree, H. Eyring, Nola McKee, and I. Cutler, Trans. Soc. Rheology **5**, 67 (1961).

[23] A. F. Gabrysh, H. Eyring, and I. Cutler, J. Am. Ceram. Soc. (to be published).

rate of formation of the cross linkage. In this case a plot of the logarithm of the viscosities at the yield point versus the reciprocal of temperature has a negative slope. Activation energies for this process are comparatively low, -1.3 kcal/mole. Both the stability and the activation energy are of the same order of magnitude and it appears that mobility of the water is the controlling factor in both cases.

In the considerations for activation energy only the 70, 54, 26, and 12°C points were used. The viscosity at 1°C ($1/T=0.0039$) varied appreciably from the straight line in all four plots of Fig. 14. The variation is perhaps caused by internal frictional heat bringing about the peak density change of water which occurs at 4°C.

II. APPARATUS FOR THE STUDY OF THE EFFECT OF HIGH PRESSURE ON THE FLOW NATURE AND THE NON-NEWTONIAN CHARACTER OF GREASES

INTRODUCTION

Investigations[24] of pressures between gear teeth and bearings have shown that lubricants in those areas are subjected to pressures of thousands of pounds per square inch and that the viscosity of the lubricants in the contact areas undergoes a marked change. To study the changes in viscosity a number of methods have been used.

In P. W. Bridgman's Laboratory, at Harvard University, Flowers[25] invented a rolling-ball viscometer with which Hersey[26,27] later investigated fats and mineral oils. Hersey and Shore[28] working in the 1000- to 4000-atm range found that, under constant temperatures, certain oils undergo apparent solidification. Sage and Lacey[29,30] used an inclined-plane "rolling-ball" apparatus where saturated solutions, under saturation pressure and temperature, showed a decrease in viscosity. Dow[31-33] studied the effects of pressure on oils with a rolling ball apparatus designed for pressures of 41 000 atm.

In 1941, Norton[34] departed from the study of Newtonian viscosity, with which the preceding investigators were concerned, and using a capillary undertook to determine the non-Newtonian character of the flow curves of oils under pressure. In general, it was found that critical rates of increase of the pressure produced either soft solids or much stiffer consistencies which behaved like plastic

greases. More recently Hahn,[35] also using a test capillary, reported on some non-Newtonian behavior of lubricating oils under pressure.

The capillary-type apparatus reported here is similar to that used by Norton and Hahn but makes use of a five-cylinder, axial-piston pump which is supercharged by a gear pump for the high pressure stage and an oil "reservoir" to completely eliminate the antagonistic pressure ripples caused by the action of a pump. The ripples were experienced in the designs of apparatus used by the previous workers. The reproducibility of the experimental results is within 2%.

CONSTRUCTION

1. General

The essential features of the apparatus are shown in Figs. 15–17. Pressure is produced in the system by a "Vanguard" Y26-A hydraulic pumping unit obtained from the Owatonna Tool Company, Owatonna, Minnesota, Fig. 16 A. The unit is specially equipped with (1) a 4-way, lever-operated, "shear-seal, open-center" type control valve, (2) a pressure gauge calibrated in psi, (3) a pressure regulating valve which bypasses oil when a predetermined pressure has been reached and which adjusts from 1000 to 10 000 psi, and (4) a 5-gallon oil reservoir. It was found that on continuous operation the oil in the reservoir became hot. The reservoir was subsequently equipped with coils through which water is circulated to cool the hydraulic fluid.

The pumping unit is connected, by a high-pressure hose, through a "T," to two parallel sets of three "oil-reservoir" tanks in series Fig. 16 C. These old oxygen and nitrogen tanks were obtained as war surplus property. The tanks are connected by high-pressure stainless steel tubing through another "T" and an oil filter (Fig. 16 B) to an OTC single acting 20-ton hydraulic ram, Fig. 16 D, whose specifications are as follows: maximum working pressure, 10 000 psi; length closed, 11 $\frac{5}{16}$ in.; length open, 16 $\frac{5}{16}$ in.; diameter of moving shaft, 2$\frac{1}{4}$ in.; oil capacity, 26 cu in.; effective ram area, 5.16 in.[2]

2. Pressure Intensification

A pressure chamber, Fig. 16 E, consists of a piston 0.750±0.001 in. in diameter. With the effective ram area of 5.16 in.[2], the pressure in the chamber is intensified about 12 times that of pump pressure. The war-surplus tanks have been tested and safely operated at a hydrostatic pressure of 5000 psi, therefore the safe operating pressure is approximately 60 000 psi. Two O-rings on the piston and one in the cylinder, Fig. 17, serve effectively as seals to

[24] C. W. Georgi, *Motor Oils and Engine Lubrication* (Reinhold Publishing Corporation, New York, 1950), p. 57.
[25] A. E. Flowers, Proc. ASTM, **14**, Part 2, 565 (1914); Trans. ASME **43**, 1269 (1921).
[26] M. D. Hersey, J. Washington Acad. Sci. **6**, 525 (1916).
[27] M. D. Hersey and G. S. Snyder, J. Rheology **3**, 298 (1932).
[28] M. D. Hersey and H. Shore, Mech. Eng. **50**, 231 (1928).
[29] B. H. Sage, Ind. Eng. Chem. **15**, 261 (1933).
[30] B. H. Sage and W. N. Lacey, Ind. Eng. Chem. **32**, 587 (1940).
[31] R. B. Dow, J. Appl. Phys. **8**, 367 (1937).
[32] R. B. Dow, M. R. Fenske, and H. E. Morgan, Ind. Eng. Chem. **29**, 1078 (1937).
[33] R. B. Dow, J. Colloid Sci. **2**, 81 (1947).
[34] A. E. Norton, M. J. Knott, and J. R. Muenger, Trans. ASME **63**, 631 (1941).

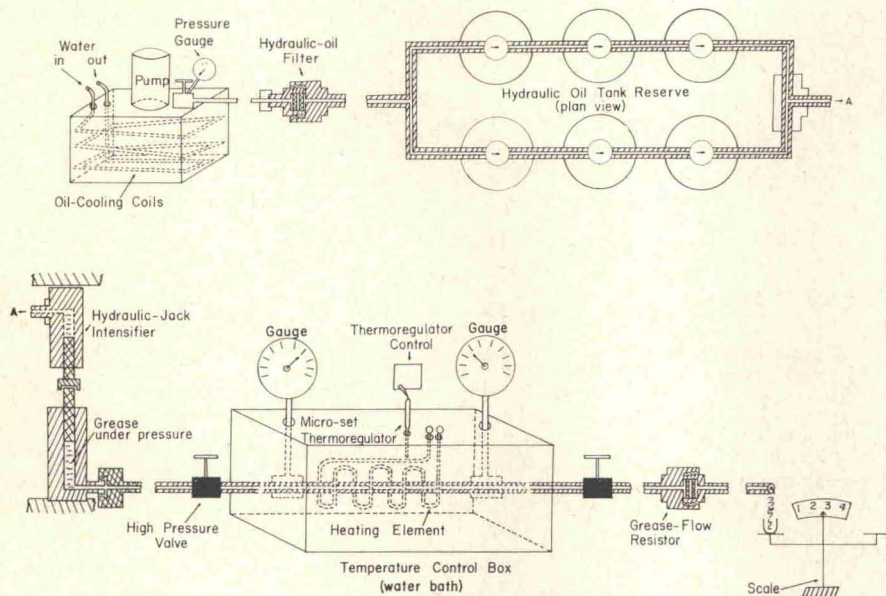[35] S. J. Hahn, H. Eyring, I. Higuchi, and T. Ree, NLGI Spokesman **22**, 121 (1958).
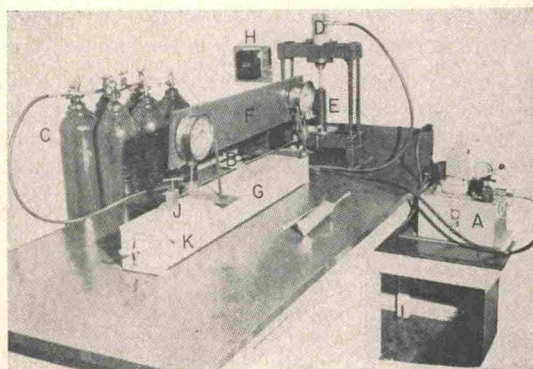
FIG. 15. Schematic of high-pressure apparatus.

FIG. 16. Photograph of apparatus: (A) model Y26-A Vanguard 5-cylinder, axial-piston pump supercharged by a gear pump, (B) hydraulic-oil filter, (C) war-surplus cylinders—oxygen and/or nitrogen —filled with hydraulic oil, (D) OTC single-acting 20-ton hydraulic ram, (E) pressure chamber, (F) pressure gauges, (G) temperature-control refrigeration (−45°C) and water bath unit, (H) thermo-regulator control, (J) high pressure valve, (K) bath water outlet.

leaks. The grease is injected with a grease gun through a port containing a ball valve.

The grease is ejected through a high-pressure stainless steel tube into a stainless steel capillary whose internal diameter is 0.083 in. The test capillary is provided with two pressure gauges, exactly 40 in. apart, for measuring the initial pressure P_i and final pressure P_f.

3. Temperature Control

The capillary is kept in a temperature controlled refrigeration (−45°C) and water bath unit (Fig. 16 G) fitted with heating coils controlled by a Micro-set thermoregulator through a thermorelay. A "reservoir" capillary coil is incorporated in the temperature control unit, just before the initial-pressure gauge, to gain thermo-equilibrium of grease in the test capillary.

MEASUREMENTS

1. Newtonian Flow

The pressure drops through the 40-in. capillary between the two gauges are obtained by controlling the initial pressure P_i and the final pressure P_f, for a constant average pressure of $(P_i+P_f)/2$. Thus, various pressure drops are obtained under the same hydrostatic pressure $(P_i+P_f)/2$.

The pressure P_i and P_f on the gauges are controlled by the pump—reserve-tank arrangement and the outlet valve (Fig. 16 J), respectively. With some greases at the higher pressures (15 to 30 000 psi) one outlet valve did not completely control fluctuation at the "final-pressure" gauge. Excellent control was achieved by putting in series with the outlet valve a coiled and a "filter" type resistance to the grease flow plus a second valve. Proper adjustment of the two valves proved to be completely satisfactory for minimizing gauge fluctuation.

The weight of grease extruded under pressure through the capillary tube during a given time interval is a measure of flow rate Q. The flow rate Q through a tube of radius r and length L at a pressure drop ΔP is converted to shear stress f and shear rate $\dot{s}$ by the following relations:

$$f = r\Delta P/2L$$
$$\dot{s} = 4Q/\pi r^3.$$

A plot of shear rates $\dot{s}$ against shear stress f shows the flow curves for a material.

2. Non-Newtonian Flow

Since 1884 investigators have worked[36,37] on theoretical relations for the non-Newtonian behavior of oils as a func-

[36] W. Warburg and S. Sachs, Am. J. Phys. **22**, 518 (1884).
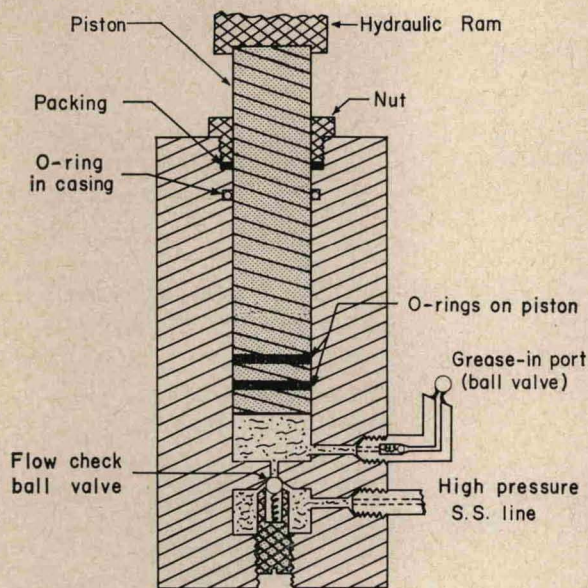[37] C. Barass, Am. J. Sci. **45**, 87 (1893).

FIG. 17. Schematic of pressure chamber.

tion of pressure. These were successively, but empirically, improved by later workers.[38-42] Ewell and Eyring[43] also Frish, Eyring, and Kincaid[44] have advanced a general theory of the effect of pressure on viscosity. The pressure effect is given as due to the volume change in passing from a normal to an activated state; e.g.,

$$\Delta F^{\ddagger} = \Delta F_1^{\ddagger} + P\langle \Delta V \rangle_{av}^{\ddagger}, \qquad (22)$$

where $\langle \Delta V \rangle_{av}$ is the average volume increase for passage from the normal to the activated state.

Present studies of the rate of shear as a function of shear stress $[\dot{s} = F(f)]$ are concerned with the flow mechanism of lubricants and high polymer solutions based on the assumptions that (a) stationary and viscous flow occurs where there is (b) no slippage on the wall and (c) the fluids are incompressible: For flow in a capillary, consider a cylindrical liquid surface of radius r and length L under a shear stress f (in dyn/cm²). For both Newtonian and non-Newtonian units, the resultant force, due to longitudinal traction, $2\pi r L f$, on the cylindrical surface of the capillary wall, must be equal to the net driving force, $\pi r^2 \Delta P$, i.e., $f = (\Delta P/2L)r$.

The rate of shear $\dot{s}$ is defined as the negative of the gradient of fluid velocity u or

$$\dot{s} = -du/dr. \qquad (23)$$

[38] H. Suge, Bull. Inst. Phys. Chem. Research (Tokyo) 12, 643 (1933).
[39] S. J. Needs, Trans. ASME 60, 347 (1938).
[40] E. K. Gatcombe, Trans. ASME 67, 177 (1945).
[41] R. B. Dow, J. S. McCartney, and C. E. Fink, J. Inst. Petrol. 27, 301 (1941).
[42] M. D. Hersey and D. B. Lowdenslager, Trans. ASME 72, 035 (1950).
[43] H. Ewell and H. Eyring, J. Chem. Phys. 5, 726 (1937).
[44] D. Frish, H. Eyring, and J. Kincaid, J. Appl. Phys. 11, 75 (1940).
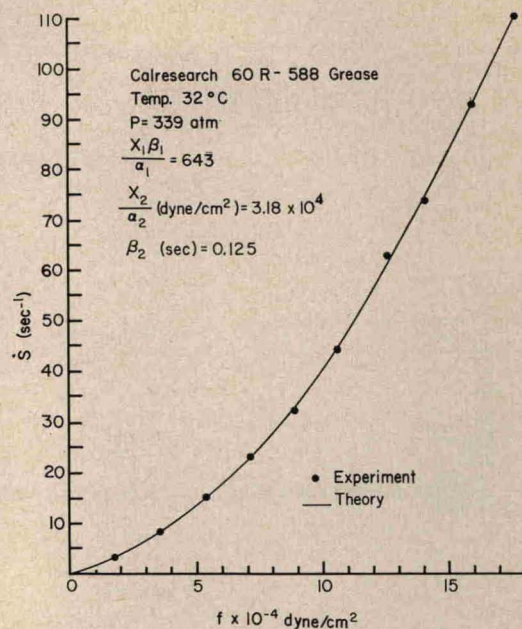
FIG. 18. Flow curve of Calresearch 60R-588 grease at 32°C.

The flow rate Q is given by

$$Q = \int_0^R \pi r^2 \dot{s} dr = 8\pi L^3/P^3 \int_0^{f_w} \phi f^3 df, \qquad (24)$$

where $f_w = RP/2L$ and is equal to the shearing stress at the wall of the capillary of radius R, and $\phi = \dot{s}/f$ is the fluidity (reciprocal of viscosity). In the Newtonian case ϕ is a constant.

Integrating Eq. (3) results in the well-known Hagen–Poiseville[45] equation $\phi = 8LQ/\pi R^4 P$. When ϕ is a function of f, as in the non-Newtonian case, $\dot{s}$ is given in terms of the flow rate as[35]

$$\dot{s} = 1/\pi R^3 [3Q + PdQ/dP]. \qquad (25)$$

The P and Q relationship is obtained from experiment, e.g., Fig. 18. Thus, all the quantities on the right side of Eq. (4) are known[46] since dQ/dP is the slope of the Q–P curve.

Based on the theory of rate processes, Eyring[47] derived an equation for a non-Newtonian system. The relation between shear stress f and shear rate $\dot{s}$ for a system composed of n flow units of different relaxation times is given by

$$f = \sum_n^\infty X_n/\alpha_n \sinh^{-1}\beta_n\dot{s}. \qquad (26)$$

[45] S. Glasstone, Physical Chemistry (D. Van Nostrand Company, Inc., Princeton, New Jersey, 1951), 2nd ed., p. 497.
[46] The capillary radius R is generally uniform. However, it has been determined that in some capillaries R varies, making it necessary to determine its "average value" by calibrating the capillary with a "standard" fluid.
[47] S. Glasstone, K. J. Laidler, and H. Eyring, The Theory of Rate Processes (McGraw-Hill Book Company, Inc., New York, 1941), pp. 477–551.

In this equation X_n is the fractional area occupied by the nth flow unit on the shear surface, $\alpha_n = (\lambda\lambda_2\lambda_3)_n/2kT$ and $\beta_n = 1/[(\lambda/\lambda_1)2k']_n$, where k is Boltzmann's constant, T the temperature, and the summation is the extension to all the flow units present. Here $\lambda_2\lambda_3$ is the cross-sectional area of a certain flow unit, λ the distance a unit moves between equilibrium positions, λ_1 the distance between planes of flow units of a certain kind, and k' the rate constant for passage of the unit over a potential energy barrier.

The experimental data of greases are explained in terms of Newtonian and non-Newtonian flow units, e.g.,

$$f = X_1\beta_1/\alpha_1\dot{s} + X_2/\alpha_2 \sinh^{-1}\beta_2\dot{s}. \tag{27}$$

The subscripts 1 and 2 refer to the Newtonian and non-Newtonian units, respectively. If it is assumed that $X_1\beta_1/\alpha_1 \ll X_2\beta_2/\alpha_2$ (the inequality is due to the fact that $\beta_1/\alpha_1 \lll \beta_2/\alpha_2$ while $X_1 \gg X_2$) then (6) becomes

$$f = X_2/\alpha_2 \sinh^{-1}\beta_2\dot{s}. \tag{28}$$

Pressure increases and decreases effect an equilibrium transition between Newtonian and non-Newtonian flow. Thus when $X_1 \gg X_2$,

$$X_2 \cong \exp(-\Delta F/RT)$$

and from (1)

$$X_2 = \exp(-\Delta F_0/RT) \exp(-P\Delta V/RT)$$
$$= K_0 \exp(-P\Delta V/RT), \tag{29}$$

where K_0 is the equilibrium constant when $P=0$. Also

$$\beta_2 = (\lambda 2k'/\lambda_1)_2^{-1} = (\lambda/\lambda_1 2kT/h)_2^{-1} \exp\Delta F^\ddagger/RT)$$
$$= \beta_{2,0} \exp(P\Delta V^\ddagger/RT, \tag{30}$$

where

$$\beta_{2,0} = (\lambda/\lambda_1 2kT/h)^{-1} \exp(F_0^\ddagger/RT).$$

Substituting Eqs. (29) and (30) into (28) yields

$$f = [K_0/\alpha_2 \exp(-P\Delta V/RT)] \sinh^{-1}$$
$$\times [\beta_{2,0} \exp(-P\Delta V^\ddagger/RT)\dot{s}], \tag{31}$$

which is the equation of flow under pressure.

By applying (31) to the $\dot{s}$-f flow curves discussed earlier, the factors X_2/α_2 and β_2 are obtained. ΔV is obtained from the slope of the line in the plot of $\ln(X_2/\alpha_2)$ against P. Similarly $\Delta V^\ddagger$ is determined from the plot of $\ln\beta$ against P. $\beta_{2,0}$ is evaluated by extrapolating the β_2 values obtained at various pressures to $P=0$. Finally, in (30), $\Delta F^\ddagger$ is readily calculated for $\lambda \cong \lambda_1$.

APPLICATION TO LUBRICANT

Figure 18 shows the theoretical and experimental flow curve for Calresearch 60R–588 grease (obtained from the California Research Corporation) under a pressure of 339 atm. The shear rate $\dot{s}$ is determined by Eq. (25) and the stress f by the relation $f = r\Delta P/2L$. The reproducibility of the experimental result is within a range of two percent. The theoretical flow curve was calculated from Eq. (27). The factors $X_1\beta_1/\alpha_1$, X_2/α_2, and β_2 were determined using Eyring's well-known method.[35]